Sonochemistry as a tool for preparation of porous metal oxides*

D. N. Srivastava, N. Perkas, A. Zaban, and A. Gedanken[‡]

Department of Chemistry, Bar-Ilan University, Ramat-Gan-52900, Israel

Abstract: The porous metal oxides are an important class of materials, because the surface area/volume ratio of a material is increased by many fold, making them very useful in surface-related applications. The mesoporous materials were discovered in the 1990s, and since then they have been excellent candidates for materials science research. These mesoporous materials are prepared by hydrolyzing the inorganic precursor (usually metal alkoxide) in an acid, basic, or neutral medium in the presence of an organic structure-directing agent, the surfactant, in a conventional method. Recently, we have demonstrated that the sonochemical technique can be employed for the synthesis of mesoporous metal oxides. The sonochemical method reduced the time period required for such synthesis by many fold, and also produced more stable structures. We got excellent results with silica, titania, yittria-stabilized zirconia (YSZ), and Fe_2O_3. We also used an inorganic precursor other than an alkoxide for the preparation of mesoporous metal oxides. In this article, we present some of the recent results on this topic.

ULTRASOUND + CHEMISTRY = SONOCHEMISTRY

Power ultrasound influences chemical reactivity through an effect known as "cavitation". Cavitation occurs by applying high-intensity ultrasound to liquids, resulting in the superimposition of sinusoidal pressure on the steady ambient pressure. Sound is transmitted through a fluid as a wave consisting of alternating compression and rarefaction cycles. In the phenomenon called cavitation, the microbubbles formed during the rarefaction cycle of the acoustic wave undergo violent collapse during the compression cycle of the wave. During the compression cycle, the bubble's content is estimated to be heated to 5000 K, and the implosion of the cavitation bubble also produced high-energy shock waves with pressures of several thousand atmospheres [1]. The ultimate consequence of the high temperature is a chemical reaction. The high pressure leads to an increased number of molecular collisions owing to enhanced molecular mobility and decreased overall volume, leading also to high chemical reactivity.

MESOPOROUS MATERIALS

The mesoporous material (MSPM) as characterized by IUPAC is the porous material having a pore diameter of $2.0 \leq d \leq 50$ nm [2]. Following the pioneering report of the hexagonal array of silica pores [3], known as MCM-41, many different-shaped mesoporous materials have been reported. The most important shapes for silica, apart from MCM-41, are cubic (MCM-48) [4] and laminar (MCM-50) [5]. MSPMs have attracted the interest of researchers owing to their commercial application in catalysis and chemical separation, as well as the challenge associated in the synthesis, characterization and process-

ing [6]. The mesoporous metal oxides are synthesized by the conventional hydrothermal method. There have been a number of models proposed to explain the formation of mesoporous materials and to provide a rational basis for the various synthesis routes. On the most common level, these models are based upon the presence of surfactants in a solution guiding the formation of the inorganic mesostructure from the solubilized inorganic precursors. Surfactants contain a hydrophilic head-group and a long hydrophobic tail-group within the same molecule and will self-organize in such a way as to minimize contact between the incompatible ends. How the inorganic precursor interacts with the surfactant is the issue whereby the models diverge; the type of interaction between the surfactant and the inorganic precursor can be seen as a significant difference among the various synthesis routes, and the resulting classes of mesoporous materials. All these aspects of the mesoporous materials have already been discussed in detail [2,5].

OUR CONTRIBUTION TO THE FIELD

For the reasons mentioned above, we have tried to extend our expertise and to apply the sonochemical technique and prepare the porous metal oxides. Sonochemistry does not affect the mechanism of the formation of mesostructure. Instead, it increases the rate of the reaction as discussed in the first section. The principal advantage of using the sonochemical technique for the preparation of porous metal oxide is that it reduced the overall duration of the process by many fold. It has been observed that this method requires only 3 h as compared to 48–72 h in other conventional methods. In addition, in the case of MCM-41, we have demonstrated that the sonochemical product was hydrothermally more stable than the corresponding sol-gel product. We have attributed this stability to the thicker walls of the sonochemical product [7]. We have already reported on the synthesis of a few mesoporous metal oxides using the sonochemical method, including silica [8], titania [9], and YSZ [10]. These results have already been reviewed elsewhere [11]. An outstanding result obtained previously is a surface area as high as 850 m^2/g measured for mesoporous titania [9].

In the current review, we present recent results related to the transition-metal oxides such as Ni [12], Co [12], Fe [13], and also Sn [14]. The general features observed for these metal oxides are that their surface area is not as high as that obtained for titania, but the surface areas are comparable with earlier reports on mesoporous Ni, Co, Fe, and Sn oxides synthesized by other methods.

METHODOLOGY

A general scheme for the synthesis of the mesoporous material by sonochemistry is given in Fig. 1. The surfactant templating method has been used for the preparation of these porous oxides in a basic medium. The inorganic precursor, the surfactant, the pH of the reaction mixture, and the surface area measured for the various products are given in Table 1. In a typical experiment, we dissolved the surfactant in a minimum amount of ethanol in a 100-mL sonication flask. The required amount of inorganic precursor was added to the surfactant solution, and then the sonication flask was further filled with distilled water [12–14,22]. The pH was maintained on the value listed in Table 1 using NH_4OH, and then the gel was sonicated for 3 h. The precipitate formed was then centrifuged, washed, and dried. The surfactant was removed either by calcination or solvent extraction. The extent of the removal of the surfactant was controlled by IR spectroscopy, examining the 2800–3000-cm^{-1} region of the CH_2 stretching modes of the alkyl chain, and by thermogravimetric analysis (TGA) measurements controlling the weight loss of the surfactant. The characterization of MSP metal oxides before and after the removal of the surfactant was conducted by powder X-ray diffraction (PXRD) measurements [12–14,22].
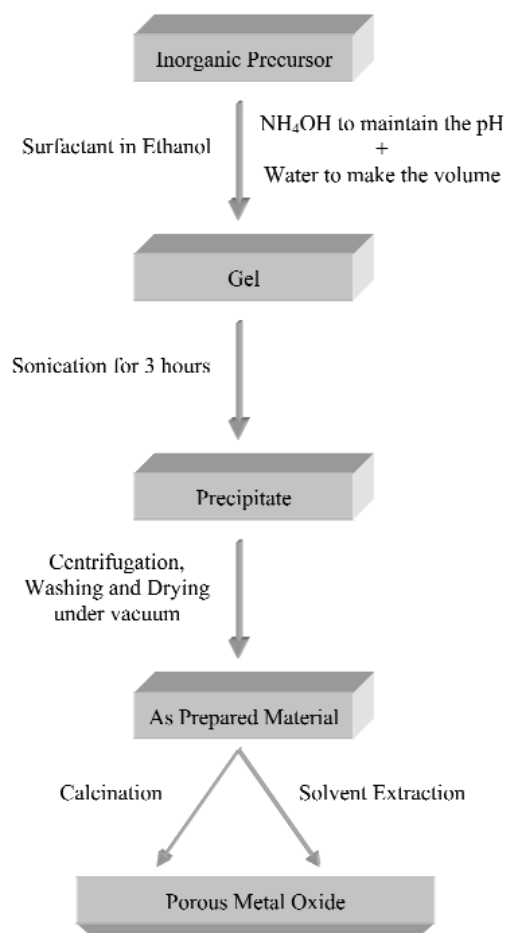
Fig. 1 Schematic presentation of the method of preparation of porous metal oxide by sonochemical technique.

Table 1 The inorganic precursor, surfactant used, pH of the medium, and surface area found for different metal oxides.

Metal oxide	Inorganic precursor	Surfactant	pH	Surface area	Reference
Fe_2O_3	Iron(III)ethoxide	CTAB	10.6	274 m^2/g	13
NiO	$Ni(OC_2H_4OCH_3)_2$	ODA	8.5	40 m^2/g	12
Co_3O_4	$[Co(acac)(OMe)(MeOH)]_4$	ODA	8.5	72 m^2/g	12
NiO	$NiSO_4.6H_2O$	CTAB	9.0	104 m^2/g	22
Co_3O_4	$Co(CH_3COO)_2$	CTAB	9.0	70 m^2/g	22
SnO_2	Tin ethoxide	CTAB	10.0	156 m^2/g	14

RESULTS

In order to examine the formation of a mesoporous metal oxide, a well-established methodology must be followed. The first step is the small-angle X-ray diffraction (XRD) pattern, followed by surface area measurements and transmission electron microscopy (TEM) photographs. These are the three most

important techniques for the characterization of the mesoporous materials. The appearance of peaks in the small-angle X-ray scattering (SAXS) is an indication for the organization of the pores. Unfortunately, we did not detect any SAXS for the four metal oxides measured. Instead, we observed an increase in the XRD counts, with a plateau from 7° to 2° (2θ value) (Fig. 2). A sharp increase in the XRD intensity was observed after the removal of the surfactant, but it did not resolve as a peak. The absence of a peak in the small-angle XRD is due to the lack of long-range ordering of the pores. The order might, however, be restricted to small narrow regions. A possible explanation for the less-organized pore structure may be the weaker electrostatic interaction between the surfactant and the inorganic species in our case, as compared with the formation of MCM-41. As discussed in the section "Mesoporous materials", the inorganic component interacts with the head-group of the surfactant and condenses into a solid continuous framework. In our case, the larger size of the metal inorganic species as compared to the silicate may restrict the proper inorganic–organic framework formation leading to a less-organized mesostructure.

A second possibility is the higher reaction rate. It has been reported that a slow rate of hydrolysis helps the better ordering of the mesostructure [5]. We have already pointed out that the local high temperatures obtained as the result of the bubble's collapse accelerate the reaction rate. The first explanation is more plausible because SAXS signals were obtained for other metal oxides despite the fast reaction rates [8–9].

Another very important method for the characterization of these porous metal oxides is the direct examination of the pore structure by TEM. A few representative TEM photographs are depicted in Fig. 3. The average particle size of these oxides is about 100–200 nm, with lots of small pores of 2–5-nm diameter. The morphology of these pores is very irregular, commonly called "wormhole-like" morphology. Thus, the direct examination also confirms the less-ordered pore morphology, supporting our hypothesis for the small-angle XRD pattern of these materials.

The third most important technique for the characterization of MSPM is mapping of pore size distribution by physisorption of gases such as N_2, O_2, and Ar. When the adsorption–desorption isotherm of N_2 at 77 K was carried out for these porous metal oxides, it was found that the isotherms were H_2 type for SnO_2, Fe_2O_3, and H_3 type for Co_3O_4, NiO according to the IUPAC classification [15]. The presence of H_2-type hysteresis indicates that the effective radii of the mesoporous bodies are inhomogeneously distributed and the effective radii of the narrow entrance are of equal size. Whereas the H_3-type hysteresis is often associated with aggregates (i.e., an assembly of particles, which are loosely coherent) having slit-shaped pore structure. The pore size distribution is obtained according to
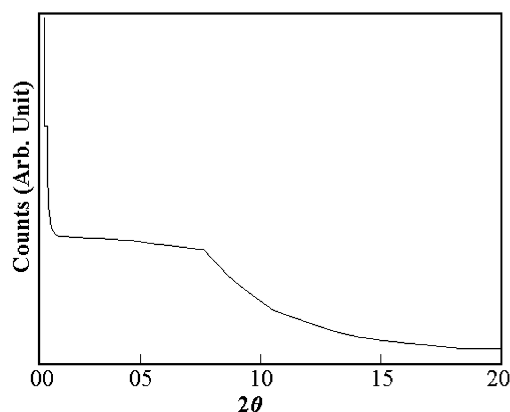

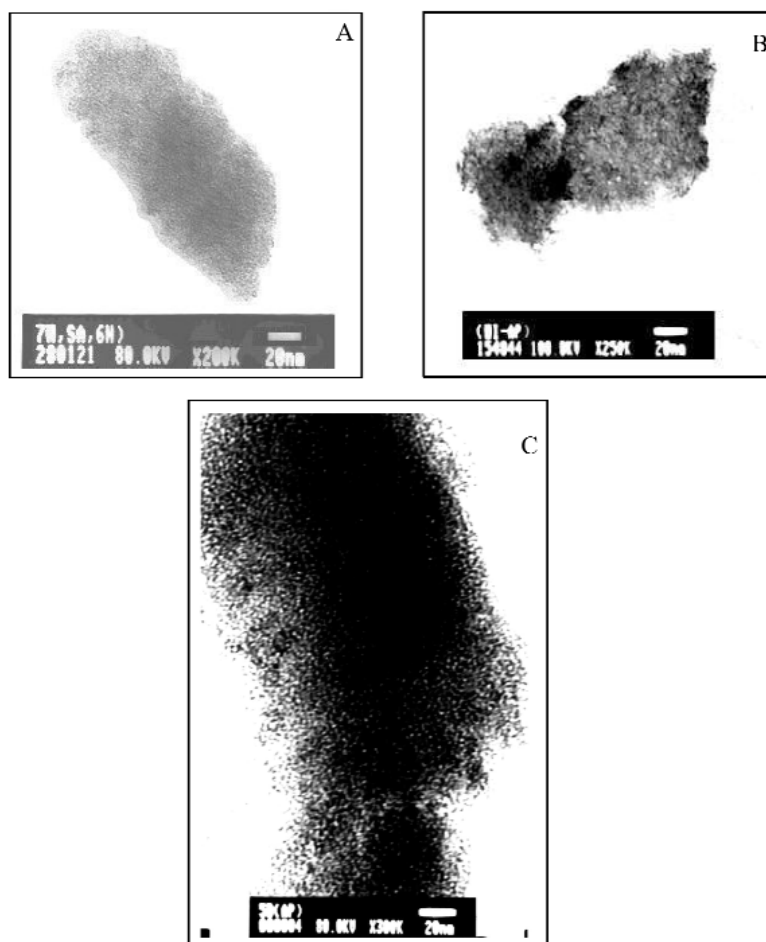**Fig. 2** Small-angle X-ray diffraction pattern for mesoporous SnO_2.

Fig. 3 TEM photographs for: (a) mesoporous Fe_2O_3 after solvent extraction; (b) as-prepared mesoporous NiO sample; (c) as-prepared mesoporous SnO_2 sample.

the Berrett-Joyner-Halenda (BJH) method using the Halsey equation for multilayer thickness [15]. These plots also confirm that the dominant peaks are in the mesoporous range. The adsorption–desorption isotherm and pore size distribution are given in Figs. 4 and 5, respectively. The calculated surface area is given in Table 1. As expected from the adsorption–desorption isotherm, the Fe_2O_3 and SnO_2 gave a higher surface area than the NiO and Co_3O_4. The relatively better pore structure (i.e., porous structure as compared to slit-like structure) in Fe_2O_3 and SnO_2, as evident by H_2 type of adsorption–desorption hysteresis, may be the reason for the better surface area in these two cases. The largest surface area has been observed for Fe_2O_3, reaching 274 m^2/g after proper solvent extraction. Unlike Fe_2O_3, where solvent extraction yielded the largest surface area, the largest surface for SnO_2 was measured after calcination reaching 156 m^2/g after calcination of 2 h at 300 ºC. The surface area of the solvent-extracted SnO_2-surfactant composite was only 92 m^2/g after extraction of 12 h.
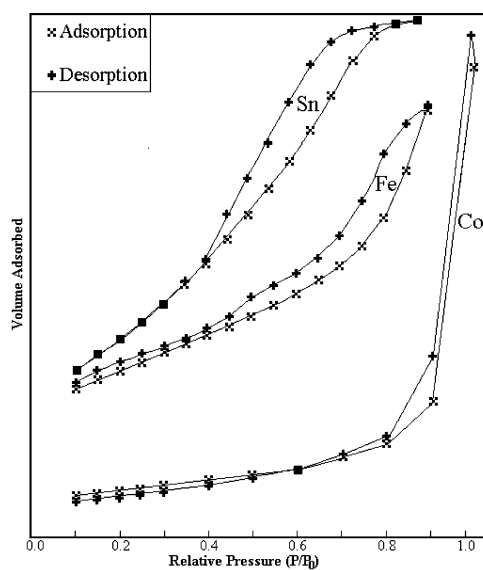
Fig. 4 Adsorption–desorption isotherm for mesoporous SnO_2, mesoporous Fe_2O_3, and porous Co_3O_4.
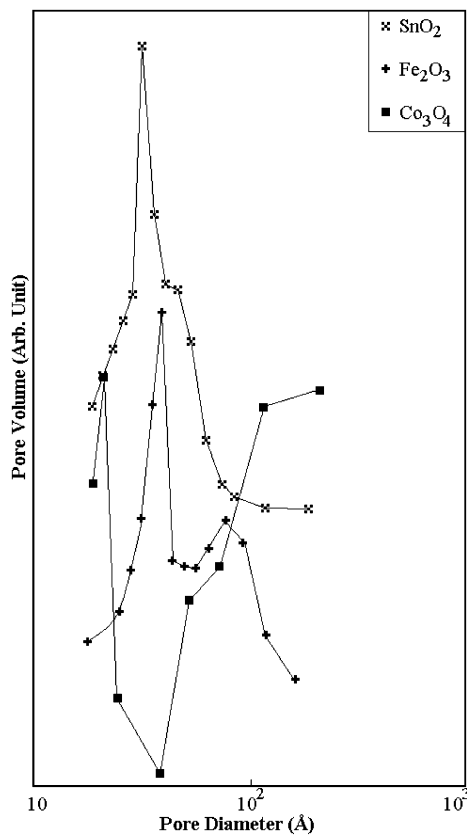

Fig. 5 Pore size distribution for mesoporous SnO_2, mesoporous Fe_2O_3, and porous Co_3O_4.

Applications

We used these materials in catalysis and dye-based solar cells. The mesoporous Fe_2O_3, when used as the catalyst in the oxidation reaction of cyclohexane under mild conditions, showed a high conversion into cyclohexanone and cyclohexanol with high selectivity. We have examined various iron-based catalysts for this reaction. The catalysts were: amorphous nanosized iron [16], iron oxide [17], $Fe_{20}Ni_{80}$ [16], and Fe_2O_3 deposited inside the pores of mesoporous titania [18]. Among all these catalysts, the Fe_2O_3 deposited inside the pores of MSP titania yielded the best result. Namely, 25.8 % of the reactant was converted into products, whereas the Ol:One ratio was 1.5:1. The Ol:One ratio is the ratio of cyclohexanol to cyclohexanone, present in the product. For mesoporous Fe_2O_3, its performance as the catalyst for the oxidation of cyclohexane was improved notably. The conversion of the cyclohexane into products was 35.6 %, while the Ol:One selectivity was 5:1. The properties of a catalyst are dependent on many factors, such as particle size, surface area, as well as the topology of the surface. The reason for observing the best catalytic results using mesoporous Fe_2O_3, may originate from the combination of these factors.

We also used porous NiO and Co_3O_4 as catalysts in the same reaction. The conversion of cyclohexane into cyclohexanone and cyclohexanol using a Ni catalyst was only in trace amount. On the other hand, the porous cobalt catalyst revealed 10 % conversion of cyclohexane into cyclohexanone and cyclohexanol. It is worth mentioning that many cobalt-based catalysts were examined for cyclohexane oxidation, such as Co powder, $Fe_{50}Co_{50}$, Co_3O_4 nanoparticles, and Fe-Co/TiO_2 [16–17]. Although the performance of the cobalt-based catalysts is not as good as iron-based catalysts, it showed a conversion of 41.1 % when amorphous Co was used in the oxidation of cyclohexane under 40 atm of oxygen (at room temperature) [16]. Under mild conditions, the maximum conversion was observed in an Fe-Co/TiO_2 alloy, which yielded 12.5 % conversion with 1.6:1 Ol:One selectivity. The performance of the mesoporous Co_3O_4 catalyst is also found to be comparable, with 10.0 % conversion and 1.5:1 Ol:One selectivity.

The porous SnO_2 has been used as an electrode material in the dye-sensitized solar cell (DSSC). The performance of the DSSC can be highly improved by using a high surface-area, wide band-gap semiconductor electrode. The nanoporous TiO_2 electrode is, so far, the most studied wide band-gap semiconductor yielding the highest solar-to-energy conversion efficiency of DSSC [19]. However, in some cases, the SnO_2 has an advantage over TiO_2 despite the lower efficiency, particularly for dyes that cannot be injected into TiO_2 owing to the energetic mismatch. The DSSC fabricated using porous SnO_2 generated a photocurrent of 5.0 mA/cm^2, which matches the current achieved with standard SnO_2-based DSSC [20].

Porous materials from an inorganic precursor other than alkoxide

Usually, metal alkoxides are used as inorganic precursor for the synthesis of mesoporous metal oxides. Owing to the lower electronegativities of the transition metals compared to the silicon, their alkoxides undergo nucleophilic reaction such as hydrolysis and condensation more readily [21]. This may be the reason that the attempts to synthesize the mesoporous oxides of transition metals using alkoxides as precursor have been mostly unsuccessful. Apart from that, the alkoxide precursors are expensive as well. Thus, we have examined some other inorganic precursor for the synthesis of porous metal oxides. We have used precursors such as $NiSO_4 \cdot 6H_2O$ and $Co(CH_3COO)_2$, with satisfactory results. The metal oxides obtained were NiO and Co_3O_4, respectively. The mesostructure was stable up to 250 ºC for both materials. The surface areas of porous NiO and Co_3O_4 measured after the removal of the surfactant by calcination at 250 ºC, were 104 m^2/g and 70 m^2/g, respectively. Further heating of the mesostructured materials led to their collapse [22]. Figure 6 shows the TEM photograph of the NiO heated up to 250 ºC for 2 h. The wormhole-like pore structure can be seen in this picture. The N_2 adsorption–desorption isotherms of these materials show the H_2 (Ni) and H_4 (Co) type of hysteresis. These results of the

Fig. 6 TEM photograph for mesoporous NiO after heating at 250 °C, prepared using $NiSO_4 \cdot 6H_2O$ as inorganic precursor.

porous metal oxides prepared from the inorganic precursor other than alkoxides are similar to those prepared from the alkoxides. We can, therefore, conclude that other inorganic precursors can also be used instead of metal alkoxide for the preparation of porous metal oxides.

ACKNOWLEDGMENTS

REFERENCES

1. T. J. Mason (Ed.). *Sonochemistry: The Uses of Ultrasound in Chemistry*, Royal Society of Chemistry, Cambridge (1990).
2. A. Corma. *Chem. Rev.* **97**, 2373 (1997).
3. C. T. Kresge, M. E. Leonowicz, W. J. Roth, J. C. Vartuli, J. S. Beck. *Nature* **359**, 710 (1992).
4. J. C. Vartuli, K. D. Schmitt, C. T. Kresge, W. J. Roth, M. E. Leonowicz, S. B. McCullen, S. D. Hellring, J. S. Beck, J. L. Schlenker, D. H. Olsen, E. W. Sheppard. *Chem. Mater.* **6**, 2317 (1994).
5. J. Y. Ying, C. P. Mehnert, M. S. Wong. *Angew. Chem. Int. Ed.* **38**, 56 (1999) and references cited therein.
6. T. J. Barton, L. M. Bull, W. G. Klemperer, D. A. Loy, B. McEnaney, M. Misono, P. A. Monson, G. Pez, G. W. Scherer, J. C. Vartuli, O. M. Yagh. *Chem. Mater.* **11**, 2633 (1999).
7. X. Tang, S. Liu, Y. Wang, W. Huang, Y. Koltypin, A. Gedanken. *Chem. Commun.* 2119 (2000).
8. Y. Wang, X. Tang, L. Yin, W. Huang, A. Gedanken. *Adv. Mater.* **12**, 1137 (2000).
9. Y. Wang and A. Gedanken. *Adv. Mater.* **12**, 1183 (2000).
10. Y. Q. Wang, L. X. Yin, O. Palchik, Y. R. Hacohen, Y. Koltypin, A. Gedanken. *Langmuir* **17**, 4131 (2001).
11. A. Gedanken, X. Tang, Y. Wang, N. Perkas, Y. Koltypin, M. V. Landau, L. Vradman, M. Herskowitz. *Chem. Eur. J.* **7**, 4546 (2001).
12. D. N. Srivastava, N. Perkas, G. A. Seisenbaeva, Y. Koltypin, V. G. Kessler, A. Gedanken. *Ultrason. Sonochem.* (2002). In press.
13. D. N. Srivastava, N. Perkas, A. Gedanken, I. Felner. *J. Phys. Chem. B* **106**, 1878 (2002).

14. D. N. Srivastava, S. Chappel, O. Palchik, A. Zaban, A. Gedanken. *Langmuir* **18**, 4160 (2002).
15. K. S. W. Sing, D. H. Everett, R. A. W. Haul, L. Moscou, R. A. Pietotti, J. Rouquerol, T. Siemienieska. *Pure Appl. Chem.* **57**, 603 (1985).
16. V. Kesavan, S. P. Sivanand, S. Chandrasekaran, Y. Koltypin, A. Gedanken. *Angew. Chem. Int. Ed.* **38**, 3521 (1999).
17. N. Perkas, Y. Koltypin, O. Palchik, A. Gedanken, S. Chandrasekaran. *Appl. Catal. A: General* **209**, 125 (2001).
18. N. Perkas, Y. Q. Wang, Y. Koltypin, A. Gedanken, S. Chandrasekaran. *Chem. Commun.* **11**, 988 (2001).
19. B. O'Regan and M. Gratzel. *Nature* **353**, 737 (1991).
20. S. Chappel and A. Zaban. *Sol. Energ. Mat. Sol. C* **71** (2), 141 (2002).
21. A. Vioux. *Chem. Mater.* **9**, 2292 (1997).
22. D. N. Srivastava, V. G. Pol, O. Palchik, A. Gedanken. *Micropor. Mesopor. Mat.* (2002). Submitted for publication.